Tavares, R., Melro, A. R., Bessa, M. A., Turon, A., Liu, W. K., & Camanho, P. (2016). Mechanics of hybrid polymer composites: analytical and computational study. Computational Mechanics, 57(3), 405-421. 10.1007/s00466-015-1252-0

**Computational Mechanics manuscript No.**
(will be inserted by the editor)

# Mechanics of hybrid polymer composites: analytical and computational study

**Rodrigo P. Tavares · António R. Melro · Miguel A. Bessa · Albert Turon · Wing K. Liu · Pedro P. Camanho**

Received: date / Accepted: date

**Abstract** Three different models with increased complexity to study the effects of hybridization on the tensile failure of hybrid composites are proposed. The first model is a model for dry bundles of fibres based on the statistics of fibre strength. The second is a model for composite materials based on the multiple fragmentation phenomenon. Lastly, a micromechanical numerical model is developed that considers a random distribution of fibres and takes into account the stochastic nature of fibre strength. This study aims to understand the controlling factors that lead to pseudo-ductility, as well as establish the sequence of failure mechanisms in hybrid composites under tensile loadings.

**Keywords** Hybrid composites · Pseudo-ductility · Analytical modelling · Numerical modelling

## 1 Introduction

Composite materials, in particular fibre-reinforced composites, play an important role in structural applications, however their use is partly hampered due to the low toughness they exhibit. Fibre hybridisation is a strategy that can lead to improved composite properties and performance, as it not only changes the material properties but also changes the damage propagation mechanisms leading to final failure [21].

The objective of this work is to study the effects of fibre hybridization on the tensile failure of unidirectional hybrid composites. Taking into account that fibre-reinforced composites are complex materials with multiple constituents it is hard to assess the effects that each of the constituent's properties have on the behaviour of composite materials, therefore, reliable models for the tensile failure of hybrid composites are essential. The first author to model hybrid composites was Zweben in 1997 [29] using an extended shear lag model for hybrid composites. In this model the composite is modelled as one dimensional arrangement of alternating Low Elongation (LE) and High Elongation (HE) fibres and it was used to determine the hybrid effect as a function of the fibres' properties. Later Fukuda [8] assessed some of the shortcomings of Zweben's model and developed a different one dimensional model, with an improved expression for the stress concentrations in hybrid composites.

More recently, Mishnaevsky and Dai [10] developed a 2D numerical fibre bundle model with a random fibre packing. Using Monte-Carlo method, random properties are given to the fibres according to a Weibull distribution. The authors also developed a 3D finite element model that was used to validate the fibre bundle model. Swolfs et al. [23] developed a model using the chain of bundles approach with a modified Weibull distribution under very local load sharing assumptions that was used to characterize the cluster development in carbon/glass hybrid composites, concluding that the

Rodrigo P. Tavares · Pedro P. Camaho
DEMec, Faculdade de Engenharia, Universidade do Porto, Rua Dr. Roberto Frias, 4200-465 Porto, Portugal
INEGI, Rua Dr. Roberto Frias, 400, 4200-465 Porto, Portugal E-mail: em10140@fe.up.pt

António R. Melro
Advanced Composites Centre for Science and Innovation (ACCIS), University of Bristol, Queen's Building, University Walk, Bristol BS8 1TR, United Kingdom

Miguel A. Bessa · Wing K. Liu
Department of Mechanical Engineering, Northwestern University, 2145 Sheridan Rd., Evanston, IL 60201, USA

Albert Turon
AMADE, Polytechnic School, University of Girona, Campus Montilivi s/n, 17071 Girona, Spain

critical cluster size is around 20 fibres and varies with the hybrid volume fraction.

Several simplified Global Load Sharing (GLS) models have been developed and used to do parametric studies on the effects of fibre hybridization in composite materials. Rajan and Curtin [16] developed a GLS theory to guide the design of fibre reinforced hybrid composites with superior mechanical properties to non-hybrid composites. The authors concluded that for hybrid composites with a low volume fraction of LE fibres it is possible to increase the composite's stiffness and pullout stress without compromising the tensile strength and strain of the material. Swolfs et al. [22] also developed a GLS model that was used for a parametric study on carbon/glass hybrid composites and achieved similar results for the hybrid effect as the ones reported in the literature.

Usually composite materials undergo catastrophic failure with a stress-strain diagram as presented in Figure 1a. Hybridizing the composite material changes the failure process which results in stress-strain diagrams similar to Figure 1b, where the two load drops correspond, respectively, to the failure of the LE fibres and the HE fibres. The objective of this work is to model the tensile failure of hybrid composites and to understand the mechanism and failure sequence in these materials. By understanding the controlling factors in the behaviour of hybrid composite materials it is possible to design a material with either an hybrid effect (Figure 1b) or with a pseudo-ductile behaviour (Figure 1c). Three different models are presented, with increasing levels of complexity. Firstly, a model for dry bundles of fibres, that does not take into account the presence of the matrix, and that is used to understand the effects of the fibre strength distribution parameters in the failure of tows of fibres is proposed. Secondly, a model based on the fragmentation of a single fibre is developed for hybrid composites. Finally, a computational micromechanical model is developed to understand the mechanisms that control the failure of hybrid composites.

## 2 Analytical models for hybrid response

### 2.1 Model for dry bundles of fibres

Failure of UD composites under tensile loading is a fibre dominated process, i.e. fibres and fibre tows are fundamental entities in composite materials. As hybridization implies interaction between fibres that present different tensile strength distributions, the study of hybrid dry bundles is important to understand the interaction phenomena that may occur due to the interaction between both fibre strength distributions.

#### *2.1.1 Model development*

The model considers a bundle of $N_t = N_{t1} + N_{t2}$ fibres of two types, 1 and 2, with a length $L$, whose tensile strength follows a Weibull [28] distribution:

$$P(\sigma) = 1 - \exp\left[-\frac{L}{L_0}\left(\frac{\sigma}{\sigma_0}\right)^m\right] , \quad (1)$$

where $P(\sigma)$ is the cumulative failure probability of a fibre with a length $L$ at a stress $\sigma$, $\sigma_0$ and $m$ the Weibull scale and shape parameters at the characteristic length $L_0$, respectively. By generating a random number between 0 and 1, representing the cumulative failure probability ($P(\sigma)$) of each fibre, the tensile strength of the fibre is determined. As the object of study are hybrid composites, two strength distributions, one for each fibre type, need to be generated, based on each fibre's tensile strength properties. As the volume fraction of each fibre is an important factor on the tensile response of the bundles it is defined for each fibre type, 1 and 2, a volume fraction such as $V_{f1} + V_{f2} = 1$.

The model assumes a Global Load Sharing (GLS), hence it is considered that there is no interaction between the fibres. Strain-controlled conditions are also assumed and the strain is incremented from zero with a pre-defined value $\Delta\varepsilon$. In each increment the stress ($\sigma_i$) in each fibre is calculated by considering the fibres as linear elastic:

$$\sigma_i = E_{fi}\varepsilon , \quad (2)$$

where $E_{fi}$ is the Young's modulus of each fibre type and $\varepsilon$ is the applied strain. When the tensile strength of a fibre is reached, the number of broken fibres of each type ($N_{bi}$) is incremented. As it is possible to have bundles with fibres of different radii the stress in the bundle is determined as:

$$\bar{\sigma} = \frac{(N_{t1} - N_{b1})\, S_{f1}E_{f1} + (N_{t2} - N_{b2})\, S_{f2}E_{f2}}{N_t\,(S_{f1}V_{f1} + S_{f2}V_{f2})}\varepsilon , \quad (3)$$

where $S_{fi} = \pi R_{fi}^2$ is the section area and $N_{ti}$ the total number of a fibres of type $i$.

The tows considered in the following analysis are composed of 500 fibres with a gauge length of 75 mm. The volume fraction of each fibre type is varied by changing the number of fibres of each type in the bundle, maintaining the number of fibres in the bundle equal to 500.

The fibre properties used for both analytical models are shown in Table 1.

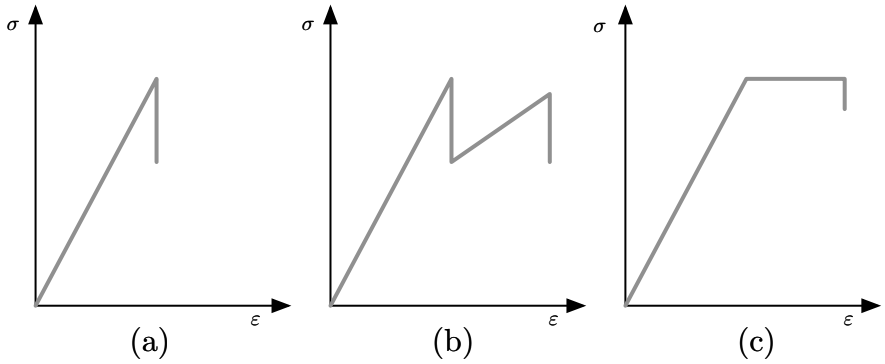


**Fig. 1** Schematic stress-strain diagrams for: (a) non-hybrid composites, (b) typical hybrid composites and (c) pseudo-ductile hybrid composites.

**Table 1** Fibre properties for the analytical models.

| Fibre | $R_f$ ($\mu$m) | $E_f$ (GPa) | $\sigma_0$ (MPa) | $m$ | $l_0$ (mm) |
|---|---|---|---|---|---|
| AS4 carbon [5] | 234 | 3.5 | 4275 | 10.7 | 12.7 |
| T300 carbon [5] | 232 | 3.5 | 3170 | 5.1 | 25 |
| M50S carbon [25] | 480 | 2.65 | 4600 | 9 | 10 |
| AR glass [7] | 70 | 7 | 1363 | 9.6 | 60 |

### *2.1.2 Results for carbon/carbon hybridization*

In this section we focus our attention on the hybridization of bundles with two types of carbon fibres. It is usual in hybrid composites to distinguish the two types of fibres as High Elongation (HE) and Low Elongation (LE), according to the failure strain they exhibit.

Considering the hybridization between the AS4 carbon fibres [5] and the T300 carbon fibres [5], whose properties are shown in Table 1. In this hybridization the T300 are the LE fibres and the AS4 the HE fibres.

The stress-strain diagrams for the tensile response of the different tows with different volume fractions of each fibre are shown in Figure 2. Analysing this figure it is possible to see that responses achieved due to hybridization are not pseudo-ductile, for either hybrid volume fractions, and that adding T300 carbon fibres to the AS4 carbon bundle reduces both the tensile strength and failure strain of the tow. Furthermore, no hybrid effect is observed.

Since the desired pseudo-ductile behavior was not achieved with this hybridization, another type of hybridization was tested, maintaining the AS4 carbon fibres as the HE fibres and using as LE fibres the M50S carbon fibres [25]. The stress-strain diagrams for this hybridization are shown in Figure 3.

Analysing this figure it is possible to conclude that for a low volume fraction of LE fibres ($V_{LE} = 0.125$ and

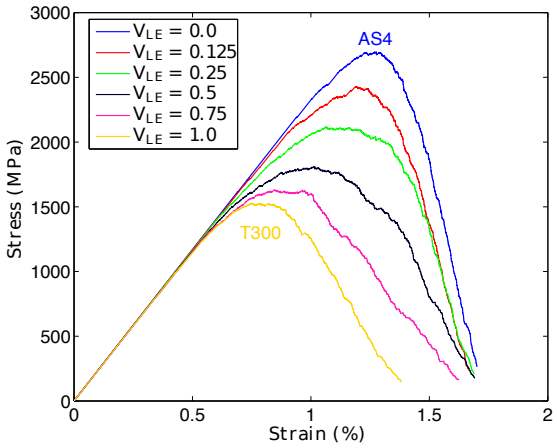


**Fig. 2** Stress-strain diagrams at various hybrid volume fractions for AS4/T300 hybridization.

$V_{LE} = 0.25$) it is possible to see what can be described as pseudo-ductility of the hybrid tow. The hybridization leads to an increase in ductility in relation to the non-hybrid LE tow, however this comes at the cost of strength and stiffness.

### *2.1.3 Results for carbon/glass hybridization*

To improve the range of available properties in hybrid composites, the hybridization between carbon and glass fibres is also analysed. The hybridization between the M50S carbon [5] fibres and the Akali Resistant (AR) glass fibres [7] results in the stress-strain diagrams shown in Figure 4.

It is observed that there is a significant difference between the behaviours of the non-hybrid tows: the M50S carbon is stiffer and stronger while the AR glass has a lower stiffness but increased ductility. This difference in

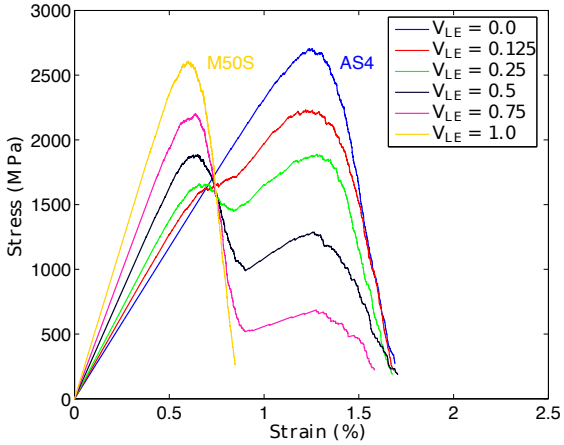


**Fig. 3** Stress-strain diagrams at various hybrid volume fractions for AS4/M50S hybridization.

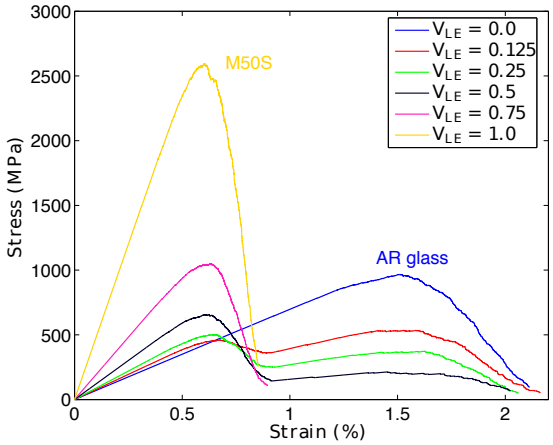


**Fig. 4** Stress-strain diagrams at various hybrid volume fractions for M50S carbon/AR glass hybridization.

stiffness of the fibres leads to a large reduction of the hybrid tows' stiffness with the addition of the glass fibres but it also potentiates the pseudo-ductile response. For a volume fraction of 0.125 of carbon fibres (LE fibres) the tow's response shows a pronounced pseudo-ductile effect, at the expense of a lower overall strength of the tow.

The above mentioned reduction of tow strength can be mitigated by selecting a different LE fibre. Replacing the M50S carbon fibres by T300 carbon fibres, presented in Section 2, it is possible to obtain the tensile response of tows shown in Figure 5.

With this hybridization it is possible to achieve a progressive failure of the bundle of fibres for a volume fraction of T300 carbon fibres equal to 0.125 and there is no load drop due to the failure of the LE fibres, as usual in hybrid composites. The pseudo-ductility is accompanied by a reduction in strength in relation to both non-hybrid, LE and HE, tows.

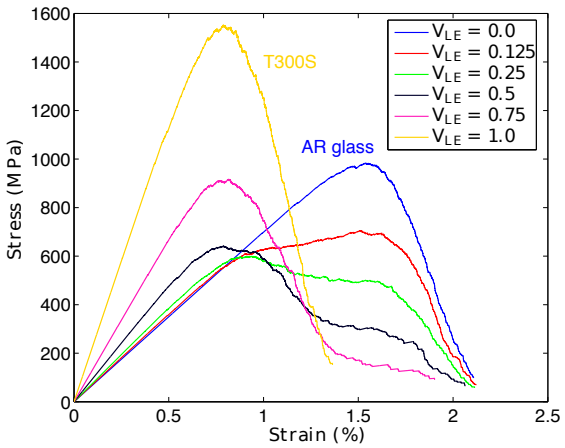


**Fig. 5** Stress-strain diagrams at various hybrid volume fractions for T300 carbon/AR glass hybridization.

### *2.1.4 Discussion*

The model for the failure of dry bundles of fibres enables to study of the effects of hybridizing tows with different types of fibres. This allows to have bundles of fibres with properties finely tuned to reach hybrid effects or pseudo-ductility.

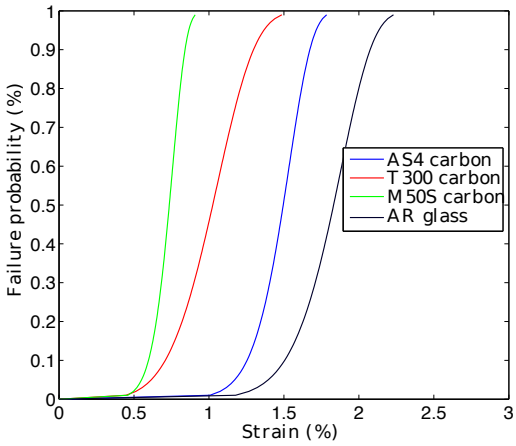


**Fig. 6** Failure strain distributions for all hybridized fibres in the fibre bundle model.

From the analysis presented herein and from others performed using realistic fibre distributions is that the pseud-ductile behavior can be achieved when there is continuity between the failure of LE and HE fibres. In other words, failure of the HE fibres should start

when failure of most, but not all, LE fibres already occurred. If this occurs then it is possible to achieve a progressive failure and, therefore, a pseudo-ductile behaviour. The failure strain distribution for the different analysed fibres are shown in Figure 6. Analysing the hybridization between the AS4 and T300 carbon fibres, curves in blue and red, respectively, it is possible to note that the failure distributions do not allow the fibres to fail progressively. This is, the HE fibres fail with similar failure strains as the LE fibres and, therefore, no pseudo-ductility is reached. Analysing the hybridization between the AS4 and M50S carbon, curves in blue and green, respectively, it is possible to see that the HE fibres begin to fail after the LE fibres have failed, which leads to the pseudo-ductile behaviour shown in Figure 4. The same behaviour can be seen for other hybridizations, leading to the conclusion that there needs to be a continuity between the failure of the LE fibres and the HE fibres to achieve a pseudo-ductile or hybrid behaviours.

## 2.2 Progressive damage model for hybrid composites

The previous model focused on the effects of the fibre strength properties on the tensile failure of fibre bundles. However, a special interest exists on the effects of hybridization in composite materials where the presence of the matrix constituent and the interface between matrix and fibres change the overall behaviour of the material. The model proposed here is an extension of the model developed by Turon et al. [26] for hybrid composites and is based on the fact that the multiple fragmentation phenomena that occurs in single fibre fragmentation tests also occurs in multiple fibre composite materials.

### *2.2.1 Single fibre fragmentation*

The fibre fragmentation model proposed by Turon et al. [26] is generalized to include more than one type of fibre. In the following, the main aspects of the model are described.

Considering that the fracture probability of a fibre of length $L$ is described by a Weibull distribution (Equation 1), it is possible to show that the average number of breaks in a fibre follows a Poisson distribution, and the average number of breaks ($\langle N \rangle$) is established, as a function of the applied stress ($\sigma$) [26]:

$$\langle N \rangle = \frac{L}{L_0} \left( \frac{\sigma}{\sigma_0} \right)^m \ . \tag{4}$$

This equation is an approximation as it does not consider that some defects are located in the stress recovery region of a fibre where the stress is lower than the applied stress. Following Turon et al. [26], if the number of breaks follows a Poisson distribution then the distance between breaks can be described by an exponential law:

$$f(x) = \Lambda e^{-\Lambda x} \ , \tag{5}$$

where $\Lambda$ is the number of breaks in a fibre per unit length

$$\Lambda = \frac{\langle N \rangle}{L} = \frac{1}{L_0} \left( \frac{\sigma}{\sigma_0} \right)^m \ . \tag{6}$$

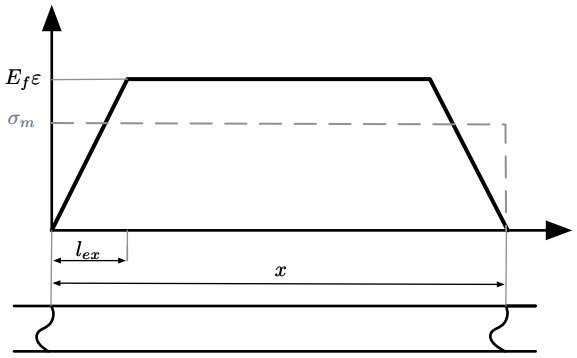


**Fig. 7** Stress profile in a fibre with multiple fractures, according to the shear-lag model.

Considering that the stress profile of a fragment of length $x$ is similar to that shown in Figure 7, the fibre has a recovery region of length $l_{ex}$ where it is not fully able to carry the applied stress [11]:

$$l_{ex} = \frac{R_f}{\tau} \frac{E_f \varepsilon}{2} \ . \tag{7}$$

Taking into account the stress profile shown in Figure 7 it is possible to define the average stress in a fragment of length $x$ as:

$$\Sigma(x) = \begin{cases} E_f \varepsilon \dfrac{x}{4 l_{ex}} \ , & x \leq 2 l_{ex} \ , \quad \text{(8a)} \\ E_f \varepsilon \left( 1 - \dfrac{l_{ex}}{x} \right) \ , & 2 l_{ex} \leq x \leq L \ , \quad \text{(8b)} \\ E_f \varepsilon \ , & x \geq L \ . \quad \text{(8c)} \end{cases}$$

The average stress in a fragmented fibre ($\sigma_m$) can be determined by integrating the axial stress in all fibre fragments within a fibre of length $L$:

$$\sigma_m = \langle N \rangle \frac{1}{L} \int x \Sigma(x) f(x) \ \mathrm{d}x \ . \tag{9}$$

The analytical solution for this integral gives the average stress in a fragmented fibre as a function of the applied strain ($\varepsilon$):

$$\sigma_m(\varepsilon) = E_f \varepsilon \left( \frac{1 - e^{-2l_{ex}\Lambda}}{2l_{ex}\Lambda} + \Lambda l_{ex} e^{-L\Lambda} \right) . \tag{10}$$

*2.2.2 Composite damage model*

To develop the damage model for the composite materials it is necessary to define how a fibre failure affects the stresses in the remaining intact fibres and to assemble the mechanical behaviour of the constituents in the composite material. As the goal of this model is to have a simple analytical model to analyse the effects of the different parameters on the tensile failure of hybrid composites a GLS model is considered. The damage model is developed in the framework of the thermodynamics of irreversible processes. The free energy of the model is defined by adding the free energy of the constituents:

$$\begin{aligned} \psi = &(1 - d_{f1})\, \psi^0_{f1}(\varepsilon_{f1})\, V_{f1} + (1 - d_{f2})\, \psi^0_{f2}(\varepsilon_{f2})\, V_{f2} \\ &+ (1 - d_m)\, \psi^0_m(\varepsilon_m)\, V_m \end{aligned} , \tag{11}$$

where $d_i$ is the damage variable, $V_i$ the volume fraction and $\varepsilon_i$ the strain of the constituent $i$, with $i$ equal to $f1$, $f2$ or $m$ depending on the constituent (type one fibre, type two fibre or matrix). The variable $\psi^0_i$ represents the free energy of the undamaged constituent, which is given by:

$$\psi^0_i = \frac{1}{2} \varepsilon^i_{ij} C^i_{ijkl} \varepsilon^i_{kl} , \tag{12}$$

where $C^i_{ijkl}$ is the constitutive tensor of the constituent $i$.

To define the composite behaviour it is necessary to define the relations between the deformation of the composite ($\varepsilon_{kl}$) and that of the constituents ($\varepsilon^i_{kl}$). That can be done by resorting to the influence tensors ($T^i_{ijkl}$) considering a serial-parallel behaviour [12, 26]. Using Equation (12) it is possible to define the free energy of the constituents as a function of the composite strains:

$$\psi^0_i = \frac{1}{2} \varepsilon_{mn} T^i_{mnij} C^i_{ijkl} T^i_{klop} \varepsilon_{op} . \tag{13}$$

The rate of dissipation $\Xi$ can be written as:

$$\Xi = \sigma_{ij} \dot{\varepsilon}_{ij} - \dot{\psi} = \left( \sigma_{ij} - \frac{\partial \psi}{\partial \varepsilon_{ij}} \right) \dot{\varepsilon_{ij}} - \sum \frac{\partial \psi}{\partial d_N} \dot{d_N} \geq 0; , \tag{14}$$

that can be simplified using the derivatives of the free energy with respect to the damage variable an the strains to

$$\Xi = V_{f1} \psi^0_{f1} \dot{d}_{f1} + V_{f2} \psi^0_{f2} \dot{d}_{f2} + V_m \psi^0_m \dot{d}_m \geq 0 . \tag{15}$$

To ensure the thermodynamic consistency the derivatives of the damage variables must be positive: $\dot{d}_{f2} \geq 0$, $\dot{d}_{f2} \geq 0$ and $\dot{d}_m \geq 0$. The constitutive equation for the damage model can be written as:

$$\sigma_{mn} = \frac{\partial \psi}{\partial \varepsilon_{mn}} = \left[ \sum (1 - d_i)\, T^i_{mnij} C^i_{ijkl} T^i_{klop} \right] \varepsilon_{op} . \tag{16}$$

As the focus of this analysis is the longitudinal failure of unidirectional hybrid composites the model can be simplified to:

$$\sigma(\varepsilon) = \left( \sum (1 - d_i) E_i V_i \right) \varepsilon . \tag{17}$$

Taking into account that the tensile failure of composite materials is mainly a fibre dominated process the damage in the matrix is not considered, meaning that the damage variable for the matrix ($d_m$) is zero for all applied strains. The damage variable for the fibres is determined from the fragmentation model (Equation 10) as:

$$d_f = 1 - \left( \frac{1 - e^{-2l_{ex}\Lambda}}{2l_{ex}\Lambda} + \Lambda l_{ex} e^{-L\Lambda} \right) . \tag{18}$$

*2.2.3 Results for carbon/carbon hybridization*

Similarly to Section 2.1.1 the results from the hybridization using two different types of carbon fibres are shown. In this section we consider the composite material to have an overall fibre volume fraction of 60% and the matrix Young's modulus ($E_m$) to be 4.6 GPa. The interfacial shear strength between the fibre and the matrix ($\tau$), necessary to determine the ineffective length (Equation 7), was considered to be equal in both fibres and equal to 50 MPa.

The first case to analysed is the hybridization between the AS4 and the T300 carbon fibres, whose stress-strain curves are shown in Figure 8.

Analysing the response it is possible to see that the T300 carbon composite has a higher failure strain and strength than the AS4 carbon composite. These results are not in agreement to what is expected from the model for dry bundles (Section 2.1.2) as the T300 fibres are the LE fibres while the AS4 are the HE fibres. Closely analysing the model it is possible to understand that the controlling parameter of the failure strain of

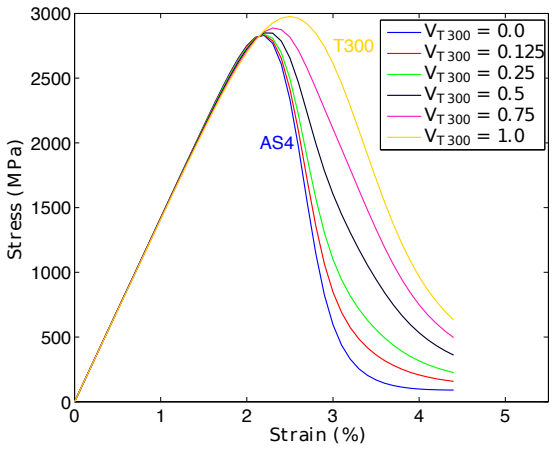


**Fig. 8** Stress-strain diagrams at various hybrid volume fractions for AS4/T300 hybridization.

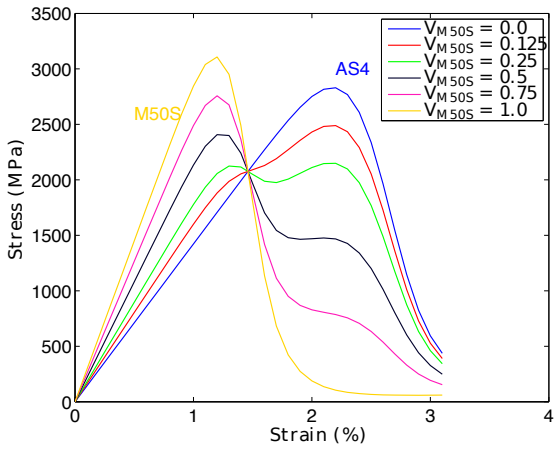


**Fig. 9** Stress-strain diagrams at various hybrid volume fractions for AS4/M50S hybridization.

the composite is a parameter that can be defined as critical strain ($\varepsilon_c$), determined based on the fibre reference strength [4], given by:

$$\varepsilon_c = \frac{1}{E_f}\left(\frac{\sigma_0^m \tau l_0}{R_f}\right)^{\frac{1}{1+m}} . \tag{19}$$

This parameter not only depends on the fibre strength parameters ($\sigma_0$ and $m$) but also the matrix-fibre interfacial shear strength ($\tau$) and the fibre radius ($R_f$). As the critical strain of the T300 carbon fibres is equal to 2.86 while that of the AS4 carbon is equal to 2.47 the failure strain of the non-hybrid T300 composite is greater than that of the AS4 composite. The initial elastic modulus of all composites with different volume fraction is very similar as both fibre types have similar Young's moduli. Similarly to what was shown in Section 2.1.2 this type of hybridization does not result in a pseudo-ductile response for any hybrid volume fraction.

The second carbon/carbon hybridization analysed with the tow model was the hybridization of the AS4 and M50S carbon fibres. Recall that this hybridization showed a clear pseudo-ductile effect for the dry bundle, so now remains the question if the matrix and interface influence the composite response significantly. Figure 9 presents the results for the composite model, where it is possible to see that for a volume fraction of M50S (LE) fibres equal to 0.25, the composite has a clear pseudo-ductile response, however, this does not occur for higher hybrid volume fractions.

### *2.2.4 Results for carbon/glass hybridization*

Similarly to what was done with the previous model, the hybridization between carbon and glass fibres is also analysed. The first hybridization shown is the hybridization between the M50S carbon fibres (LE fibres) and the Akali Resistance (AR) glass fibres (HE fibres), whose stress-strain curves for several hybrid volume fractions are shown in Figure 10.

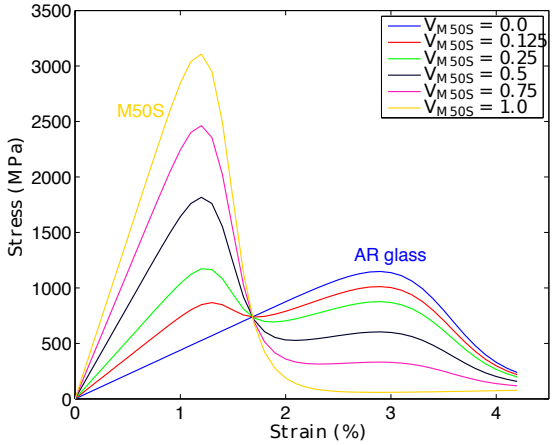


**Fig. 10** Stress-strain diagrams at various hybrid volume fractions for M50S carbon/AR glass hybridization.

The results shown are in agreement with those from the fibre bundle model (Section 2.1.3) and for a volume fraction of LE fibres equal to 0.125 it is possible to achieve a pseudo-ductile behaviour. Comparing the curve of the hybrid composite with a volume fraction of LE fibres equal to 0.125 (in red) and the non-hybrid glass composite (in blue) it is observed that the composite has an increased stiffness, due to the introduction of the stiffer carbon fibres but has a similar failure strain as the one of the non-hybrid glass composite.

This fact is accompanied only by a small decrease in tensile strength, approximately 10%.

The hybridization between the T300 carbon and the AR glass fibres lead to a pseudo-ductile response in the tow model (Section 2.1.3). The results for this hybridization, using the proposed composite damage model, are shown in Figure 11.

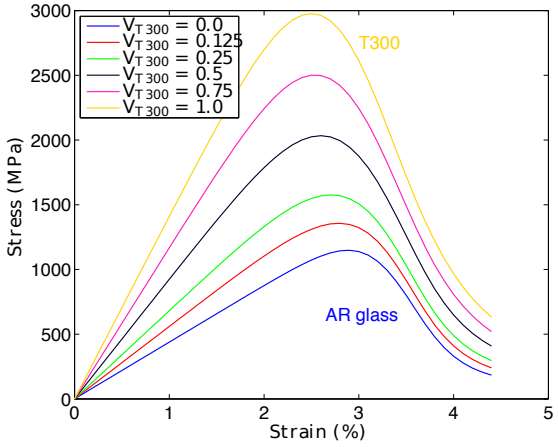


**Fig. 11** Stress-strain diagrams at various hybrid volume fractions for T300 carbon/AR glass hybridization.

The results for this type of hybridization are not in accordance with the results for the fibre bundle model as pseudo-ductile behaviour was not achieved. Analysing the critical strains of both fibre types, it is seen that the value for the T300 carbon fibres is 2.86 while that for the AR glass fibres is 3.28. As these values are close, it is seen that the failure strains of both non-hybrid composites are similar and, therefore, hybridization does not lead to the desired pseudo-ductile or hybrid behaviour.

### *2.2.5 Discussion*

Analysing the same hybridizations as in Section 2.1 it is observed that the results differ. Some materials present the same pseudo-ductile behaviour seen in the fibre bundles. However, this is not the case for all materials. It is concluded that to achieve pseudo-ductility it is necessary that the failure strains and, therefore, the critical strains ($\varepsilon_c$) of both non-hybrid composites must be different from each other. If this happens, the hybridization leads to a pseudo-ductile or hybrid behaviours and a non-catastrophic failure of the hybrid composite is achieved, usually, for low volume fractions of LE fibres. The tensile strength and failure strain, as well as the stiffness of the hybrid composite will depend on the properties of both fibre types and on the hybrid volume fraction.

## 3 Direct numerical simulation of longitudinal tensile fracture of hybrid composites

The analytical models are useful to understand the effects of some key parameters on the tensile failure of hybrid composites, however they are still unable to capture all the mechanisms of failure that occur in this type of composite materials. To do so it is necessary to resort to direct numerical simulation, namely micro-scale numerical models that are able to distinguish the behaviour of the various components and accurately represent the interaction between them.

In the micro-scale numerical models it is necessary to develop a Representative Volume Element (RVE) that is able to represent the material response. Several authors [9, 17, 23] have studied the development of clusters of broken fibres, which are the main mechanism that trigger failure of unidirectional composites loaded in the longitudinal direction. As this cluster development needs to be captured in the RVE and is usually considered to be composed of around 20 fibres, it was decided that the RVE would have in the fibre's transverse direction a length equal to 15 times the fibre radius. In the longitudinal direction it is necessary that the RVE captures the full extent of the ineffective length in a broken fibre. This lead to the choice of a longitudinal size for the RVE also equal to 15 times the fibre radius. The fibre generation in the RVE was done using a modified version of the random fibre generator developed by Melro et al. [13] to accurately represent the real microstructure of a composite material. The generated RVEs have approximately 3 million elements and are composed of Abaqus® C3D8R and C3D6R elements [19].

As there are different constituents in a composite material it is necessary to define different damage models for each that are able to accurately capture the response and failure of these materials. These are described in the following subsections.

### 3.1 Fibre damage model

The fibres are considered to be linear elastic up to failure and to have a transversely isotropic behaviour. The complementary free energy is defined as:

$$\begin{aligned}\mathscr{G}_f =& \frac{\sigma_{11}^2}{2E_1\left(1-d_f\right)} + \frac{\sigma_{22}^2+\sigma_{33}^2}{2E_2\left(1-d_f\right)} \\ &- \frac{\nu_{12}}{E_1}\left(\sigma_{11}\sigma_{22}+\sigma_{11}\sigma_{33}\right) - \frac{\nu_{23}}{E_2}\sigma_{22}\sigma_{33} \\ &+ \frac{\sigma_{12}^2+\sigma_{13}^2}{2G_{12}\left(1-d_f\right)} + \frac{\sigma_{23}^2}{2G_{23}\left(1-d_f\right)}\,,\end{aligned} \tag{20}$$

where $E_1$ and $E_2$ are the longitudinal and transverse Young's moduli, $G_{12}$ and $G_{23}$ the longitudinal and transverse shear moduli and $d_f$ is the damage variable for the fibres. To ensure that the damage process is irreversible it is necessary to guarantee that the rate of change of the complementary free energy density is greater than the externally applied stress:

$$\dot{\mathscr{G}}_f - \dot{\boldsymbol{\sigma}} : \boldsymbol{\varepsilon} = \left( \frac{\partial \mathscr{G}_f}{\partial \boldsymbol{\sigma}} - \boldsymbol{\varepsilon} \right) : \dot{\boldsymbol{\sigma}} + \frac{\partial \mathscr{G}_f}{\partial d_f} \dot{d}_f \geq 0 \, . \tag{21}$$

To ensure a positive dissipation of mechanical energy it is necessary for the strain tensor to be equal to the derivative of the complementary free energy density with respect to the stress tensor,

$$\boldsymbol{\varepsilon} = \frac{\partial \mathscr{G}_f}{\partial \boldsymbol{\sigma}} \, . \tag{22}$$

The compliance tensor ($\boldsymbol{H_f}$) can be defined as:

$$\boldsymbol{H_f} = \frac{\partial^2 \mathscr{G}_f}{\partial \boldsymbol{\sigma}^2} \, . \tag{23}$$

Inverting the compliance tensor results in the stiffness tensor ($\boldsymbol{C_f}$). The damage activation function can be defined as:

$$F_f^d = \phi_f^d - r_f \leq 0 \, , \tag{24}$$

where $\phi_f^d$ is the loading function

$$\phi_f^d = \frac{\tilde{\sigma}_{11}}{X_f^t} \, , \tag{25}$$

and $r_f$ the internal variable

$$r_f = \max \left\{ 1, \max_{t \to \infty} \left\{ \phi_{f,t}^d \right\} \right\} \, . \tag{26}$$

The loading function is function of the fibre tensile strength ($X_f^t$), which has a stochastic value and will vary from element to element. The loading function is also a function of the effective longitudinal stress $\tilde{\sigma}_{11}$, that is a component of the effective stress tensor given by:

$$\tilde{\boldsymbol{\sigma}} = \left( \boldsymbol{H_f^0} \right)^{-1} : \boldsymbol{\varepsilon} \, , \tag{27}$$

where $\boldsymbol{H_f^0}$ is the compliance tensor of the undamaged material.

To avoid mesh dependency problems and to control the energy dissipated in the fracture process, Bažant's crack band model [2] was implemented. The dissipated energy for the fibres is defined as:

$$\Psi_f = \int_0^\infty Y_f \dot{d}_f \, \mathrm{d}t = \int_1^\infty \frac{\partial \mathscr{G}_f}{\partial d_f} \frac{\partial d_f}{\partial r_f} \, \mathrm{d}r_f = \frac{G_{ff}}{l^e} \, , \tag{28}$$

where $G_{ff}$ is the fracture toughness of the fibres in mode I, $l^e$ the element's characteristic length and $Y_f$ is the thermodynamic force associated with the variable $d_f$. Using the complementary free energy for the fibres, given by (20), it is possible to define $Y_f$ as:

$$\begin{aligned} Y_f &= \frac{\partial \mathscr{G}}{\partial d_f} \\ &= \frac{1}{(1-d_f)^2} \left[ \frac{\sigma_{11}^2}{2E_1} + \frac{\sigma_{22}^2 + \sigma_{33}^2}{2E_2} + \frac{\sigma_{12}^2 + \sigma_{13}^2}{2G_{12}} + \frac{\sigma_{23}^2}{2G_{23}} \right] \, , \end{aligned} \tag{29}$$

that is always positive. The damage evolution law defined for the fibres is given by:

$$d_f = 1 - \frac{e^{A_f (1 - r_f)}}{r_f} \, , \tag{30}$$

where $A_f$ is a parameter that must be computed for each element of the mesh. The derivative of the damage law in order to $r_f$ is given by:

$$\frac{\partial d_f}{\partial r_f} = \frac{e^{A_f (1 - r_f)}}{r_f} \left( A_f + \frac{1}{r_f} \right) . \tag{31}$$

In order to solve Equation (28) it is necessary to define the relation between the real stress tensor and the effective stress tensor. This is done by imposing the principle of strain equivalence:

$$\left. \begin{aligned} \boldsymbol{\sigma} &= \boldsymbol{C_f} : \boldsymbol{\varepsilon} \\ \tilde{\boldsymbol{\sigma}} &= \boldsymbol{C_f^0} : \boldsymbol{\varepsilon} \end{aligned} \right\} \boldsymbol{\sigma} = \boldsymbol{C_f} : \left( \boldsymbol{C_f^0} \right)^{-1} : \tilde{\boldsymbol{\sigma}} = \boldsymbol{C_f} : \boldsymbol{H_f^0} : \tilde{\boldsymbol{\sigma}} \, , \tag{32}$$

where $\boldsymbol{C_f^0}$ is the undamaged stiffness tensor.

If the particular case of uniaxial tensile loading is considered, the effective stress tensor ($\tilde{\boldsymbol{\sigma}}$) is given by:

$$\tilde{\boldsymbol{\sigma}} = \begin{bmatrix} \tilde{\sigma}_{11} \\ 0 \\ 0 \\ 0 \\ 0 \\ 0 \end{bmatrix} \, . \tag{33}$$

For this stress state the three normal components of the real stress tensor are:

$$\sigma_{11} = \frac{1 - d_f}{\Delta} \left[ 1 - \beta^2 - 2\gamma \left( 1 + \beta \right) \right] \tilde{\sigma}_{11} \, , \tag{34a}$$

$$\sigma_{22} = \sigma_{33} = -\frac{1 - d_f}{\Delta} \nu_{12} \left( 1 + \beta \right) d_f \tilde{\sigma}_{11} \, , \tag{34b}$$

where

$$\beta = \nu_{23}\left(1 - d_f\right) \ , \tag{35a}$$

$$\gamma = \nu_{12}\nu_{21}\left(1 - d_f\right) \ , \tag{35b}$$

$$\Delta = \left(1 - \beta\right)\left[1 - \beta - 2\gamma\left(1 - d_f\right)\right] \ . \tag{35c}$$

The remaining shear components of the tress tensor are equal to zero. Using Equations (34) in Equation (29) results in:

$$\frac{\partial \mathscr{G}}{\partial d_f}^{UN} = \frac{\left(1+\beta\right)^2}{2E_1\Delta^2}\left[\left(1-\beta-2\gamma\right)^2 + 2\nu_{12}\nu_{21}d_f^2\right]\tilde{\sigma}_{11}^2 \ , \tag{36}$$

for the uniaxial tensile state. The damage activation function for the uniaxial tensile state is given by:

$$F_f^{dUN} = \frac{\tilde{\sigma}_{11}}{X_f^t} - r_f \leq 0 \ , \tag{37}$$

and for the damage to propagate, this equation needs to be equal to zero. Solving this equation in order to the applied effective stress results in

$$\tilde{\sigma}_{11} = X_f^t r_f \ . \tag{38}$$

Using (36), (34) and (38) in (29) results:

$$\int_0^\infty \frac{{X_f^t}^2 r_f^2\left(1+\beta\right)^2}{2E_1\Delta}\left[\left(1-\beta-2\gamma\right)^2+2\nu_{12}\nu_{21}d_f^2\right]\frac{\partial d_f}{\partial r_f}\,\mathrm{d}r_f = \frac{G_{ff}}{l^e} \ , \tag{39}$$

which needs to be solved numerically along the damage evolution law (Equation 30) to determine the parameter $A_f$, as a function of the varying element's length ($l^e$) and tensile strength ($X_f^t$).

As the tensile strength of the fibres is a stochastic parameter a random strength is assigned to each element that represents the fibre. This is done by generating random numbers ($X$) in the range 0 to 1 and by using the Weibull distribution (Equation 1) it is possible to calculate the random tensile strength:

$$X_f^t = \sigma_0\left[-\frac{L_0}{L}\ln\left(1-X\right)\right]^{1/m} \ . \tag{40}$$

### 3.2 Matrix and fibre/matrix interface modelling

The matrix is modelled using the model proposed by Melro et al. [14]. The matrix is considered to have a non-linear behaviour controlled by a paraboloidal yield criterion, being the yield surface defined as:

$$\Phi\left(\boldsymbol{\sigma}, \sigma_c, \sigma_t\right) = 6J_2 + 2I_1\left(\sigma_c - \sigma_t\right) - 2\sigma_c\sigma_t \ , \tag{41}$$

where $\sigma_c$ and $\sigma_t$ are, respectively, the compressive and tensile yield strengths of the matrix material, $J_2$ is the second invariant of the deviatoric tensor and $I_1$ the first invariant of the stress tensor. The model considers a non-associative flow rule to correctly define the volumetric deformation in plasticity. The hardening laws have been defined using Fiedler et al. [6] experimental data. The hardening laws are defined as dependent of the equivalent plastic strain for the compressive and tensile yield strengths, as these are the only strengths needed to define the yield surface. A general return mapping algorithm with an elastic predictor/plastic corrector strategy is used for the numerical implementation of the model.

The model also considers isotropic damage for the matrix, using a single damage variable that affects the stiffness of the material. The complementary free energy is defined as:

$$\begin{aligned}\mathscr{G}_m =& \frac{\sigma_{11}^2 + \sigma_{22}^2 + \sigma_{33}^2}{2E_m\left(1-d_m\right)} - \frac{\nu_m}{E_m}\left(\sigma_{11}\sigma_{22} + \sigma_{22}\sigma_{33} + \sigma_{33}\sigma_{11}\right) \\ &+ \frac{1+\nu_m}{E_m\left(1-d_m\right)}\left(\sigma_{12}^2 + \sigma_{13}^2 + \sigma_{23}^2\right) + \mathscr{G}_m^p \ ,\end{aligned} \tag{42}$$

where $d_m$ is the damage variable, $E_m$ and $\nu_m$ are, respectively, the Young's modulus and Poisson coefficient of the matrix. $\mathscr{G}_m^p$ represents the contribution of the plastic flow to the stored energy. The damage activation is controlled by a paraboloidal surface similar to the one for yielding, but considering the tensile ($X_m^t$) and compressive ($X_m^c$) failure strengths instead of the yield strengths. The damage activation is defined as:

$$F_m^d = \phi_m^d - r_m \leq 0 \ , \tag{43}$$

where $r_m$ is an internal variable controlled by a damage evolution law and $\phi_m^d$ is the loading function

$$\phi_m^d = \frac{3\tilde{J}_2}{X_m^c X_m^t} + \frac{\tilde{I}_1\left(X_m^c - X_m^t\right)}{X_m^c X_m^t} \ , \tag{44}$$

where $\tilde{J}_2$ and $\tilde{I}_1$ are the invariants of effective stress tensor ($\tilde{\boldsymbol{\sigma}}$).

The damage evolution can be measured by the rate of energy dissipation per unit volume:

$$\Xi = \frac{\partial \mathscr{G}_m}{\partial d_m}\dot{d}_m = Y_m\dot{d}_m \geq 0 \ , \tag{45}$$

where $Y_m$ is the thermodynamic force that is always positive from the definition of complementary free energy, therefore, to guarantee the condition of irreversibility, the condition $\dot{d}_m \geq 0$ is sufficient. To distinguish loading and unloading situations Kuhn-Tucker conditions must be applied, that can be defined as function of the internal variable and damage activation function.

To avoid mesh dependency issues, Bažant's crack band model [2] was implemented. The computed dissipated energy is regularized by the element's characteristic length ($l^e$):

$$\Psi_f = \int_0^\infty Y_f \dot{d}_f \, \mathrm{d}t = \int_1^\infty \frac{\partial \mathscr{G}_f}{\partial d_f} \frac{\partial d_f}{\partial r_f} \, \mathrm{d}r_f = \frac{G_{fm}}{l^e} \, , \quad (46)$$

where $G_{fm}$ is the energy release rate of the matrix material.

The damage evolution law considered can be defined as.

$$d_m = 1 - \frac{e^{A_m\left(3-\sqrt{7+2r_m^2}\right)}}{\sqrt{7+2r_m^2}-2} \, , \quad (47)$$

where $A_m$ is a parameter that is computed by solving Equation (46) for each element as function of its characteristic length.

Both the model for the matrix and the one for the fibres were implemented using Abaqus® VUMAT subroutine [19].

The fibre-matrix interface is modelled using Abaqus® surface-based cohesive behaviour [19]. Mode dependent cohesive strengths are considered, and the rate of damage progression is controlled by the fracture toughness under mode I, mode II, or mixed-mode, according to the BK law [3].

The matrix and fibre-matrix interface properties used in all the micromechanical simulations are the same and are shown in Tables 2 and 3, respectively. The resin used was Toho#113 characterized by Fielder et al. [6]. The plastic Poisson coefficient considered is a standard for epoxy resins and the fracture toughness is based on the values reported in the literature [1, 15].

The parameters for the cohesive behaviour of the fibre-matrix interfaces are based on the experimental data [27] and also on previous micromechanical simulations [1, 15] and are shown in Table 3.

**Table 2** Epoxy matrix properties.

| Material property | Value |
|---|---|
| *Young's modulus* | |
| $E_1$ (MPa) | 3760 |
| *Poisson's ratio* | |
| $\nu$ | 0.39 |
| *Coefficient of thermal expansion* | |
| $\alpha$ ($^\circ\mathrm{C}^{-1}$) | $-58 \times 10^{-6}$ |
| *Plastic Poissons ratio* | |
| $\nu_p$ | 0.3 |
| *Critical energy release rate* | |
| $G_m$ (N/mm) | 0.09 |
| *Strengths* | |
| $\sigma_{Y_T}$ (MPa) | 94.9 |
| $\sigma_{Y_C}$ (MPa) | 220 |

**Table 3** Fibre-matrix interface properties.

| Material property | Value |
|---|---|
| *Interface maximum strengths* | |
| $\tau_1$ (MPa) | 50 |
| $\tau_2$ (MPa) | 70 |
| $\tau_3$ (MPa) | 70 |
| *Interface critical energy release rates* | |
| $G_{Ic}$ (N/mm) | 0.002 |
| $G_{IIc}$ (N/mm) | 0.006 |
| $G_{IIIc}$ (N/mm) | 0.006 |
| *Mixed-mode interaction parameter* | |
| $\eta$ | 1.45 |

### 3.3 Results for the AS4 non-hybrid composite

This section is dedicated to the study of the tensile failure of the non-hybrid composite composed of AS4 carbon fibres, whose properties were determined based on the work of several authors [5, 20, 25] and are shown in Table 4.

The fibre strength determined for each element of the fibre is function of the length ($L$) considered, i.e, the length of the RVE in the fibre direction. To study the effect of the length on both the fibre strength and in the failure mechanisms, RVEs having the same fibre distribution but with different lengths were generated. Another RVE, with a length equal to 15 times the fibre radius, was generated without cohesive surfaces between the fibres and the matrix and, therefore, assuming a perfect bond between these. All these RVEs have dimensions in the direction perpendicular to the fibres equal to 15 times the fibre radius. The stress-strain curves of these non-hybrid RVE's subjected to tensile loadings in the fibre direction are shown in Figure 12.

From the presented results it is observed that the stress-strain curves are very similar for the RVEs with a length of 15 and 30 times the fibre radius. However, the RVE with a length of 45 times the fibre radius failed prematurely, which can be related with random events in the generation of the tensile strength of the elements. This leads to the conclusion that using the length of the RVE as scaling factor for the Weibull distribution is accurate as the RVEs with different length have similar failure strengths. The RVE modelled without the cohe-

**Table 4** AS4 carbon fibre properties.

| Material property | Value |
|---|---|
| *Fibre diameter* | |
| $2R$ (mm) | 0.007 |
| *Young's moduli* | |
| $E_1$ (MPa) | 234000 |
| $E_2$ (MPa) | 15000 |
| *Poissons ratio* | |
| $\nu_{12}$ | 0.2 |
| *Shear moduli* | |
| $G_{12}$ (MPa) | 15000 |
| $G_{23}$ (MPa) | 7000 |
| *Coefficients of thermal expansion* | |
| $\alpha_{11}$ ($^{\circ}C^{-1}$) | $-0.5 \times 10^{-6}$ |
| $\alpha_{22}$ ($^{\circ}C^{-1}$) | $15 \times 10^{-6}$ |
| *Critical energy release rate* | |
| $G_{ff}$ (N/mm) | $4 \times 10^{-3}$ |
| *Weibull parameters* | |
| $\sigma_0$ (MPa) | 4275 |
| $m$ | 10.7 |
| $l_0$ (mm) | 12.7 |

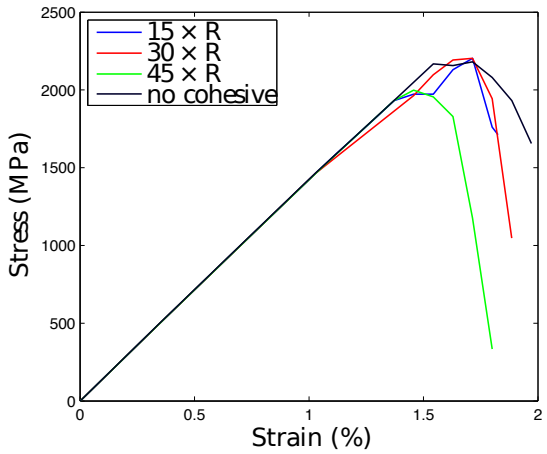


**Fig. 12** Comparison of the tensile behaviour of AS4 non-hybrid composite for different RVE's.

sive surfaces at the fibre-matrix interface shows similar failure strength as those with cohesive surfaces, however, using cohesive surfaces represent more accurately the failure mechanisms as the decohesion of the fibre-matrix interface is more realistically captured. In the RVEs with cohesive surfaces, the decohesion is observed causing the separation of the fibre from the matrix (Figure 13d). For the RVE without the cohesive surfaces, the matrix that surrounds a broken fibre is fully damaged, which creates a separation of both constituents, as the elements that are fully damaged are removed from the model. This, although leading to similar results, is inaccurate as the separation of the fibre from the matrix most often occurs not due to the cracking and failure of the matrix but due to failure of the interfaces. In Figure 13a the strength distribution of an AS4 fibre is presented. It can be observed that the tensile strength is randomly distributed simulating the presence of initial flaws or defects.

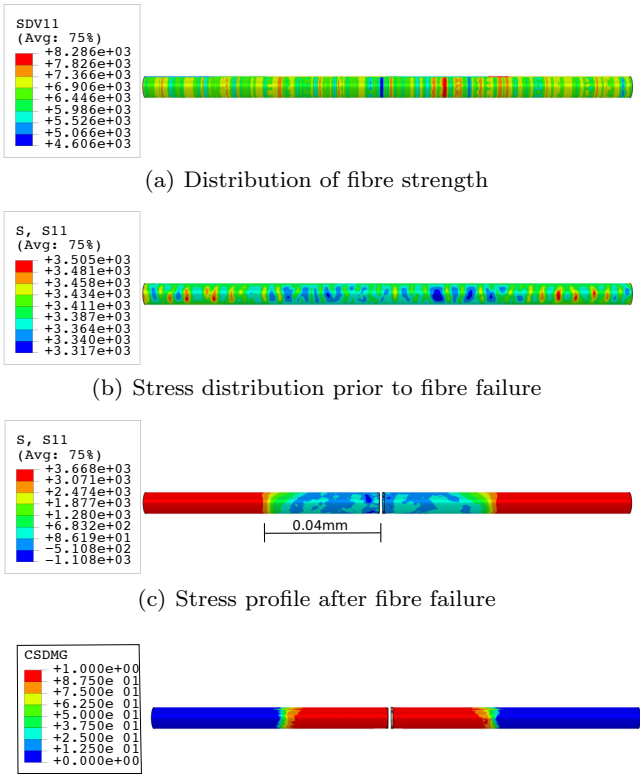


(a) Distribution of fibre strength

(b) Stress distribution prior to fibre failure

(c) Stress profile after fibre failure

(d) Interfacial damage after fibre failure

**Fig. 13** Failure process in an AS4 carbon fibre.

For the AS4 composite, as the fibres have higher failure strain than the matrix,damage development in the matrix prior to the first fibre failure is observed. This causes some stress concentrations in the fibres in the locations where the matrix is damaged which increases the failure probability in these locations, as represented in Figure 13b. However, analysing the failure locations in multiple simulations, it is observed that the main factor controlling the location of fibre failure is not stress concentrations but the location of the defects, that are simulated as elements with lower failure strength. This is seen not only to dominate first fibre failure but also the subsequent failures.

It has been observed that when a fibre fails, the fibre unloads suddenly causing a dynamic effect. The propagation of the stress wave after a fibre break can induce compression stresses in the fibres, which is captured by the model. This makes the fibre lose the load carrying capacity in some of its length, the ineffective

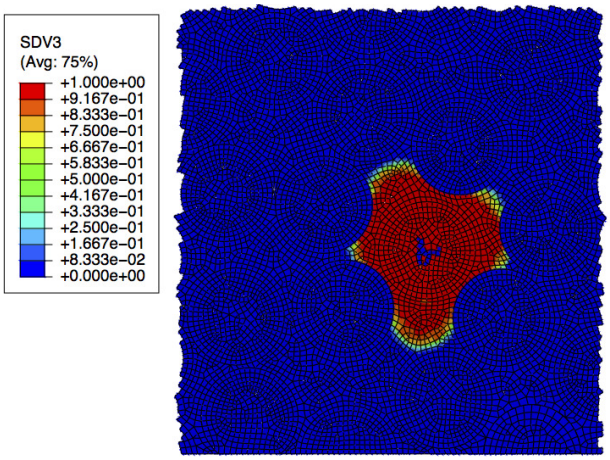


**Fig. 14** Matrix crack surrounding a broken fibre (red regions with SDV3 equal to 1).

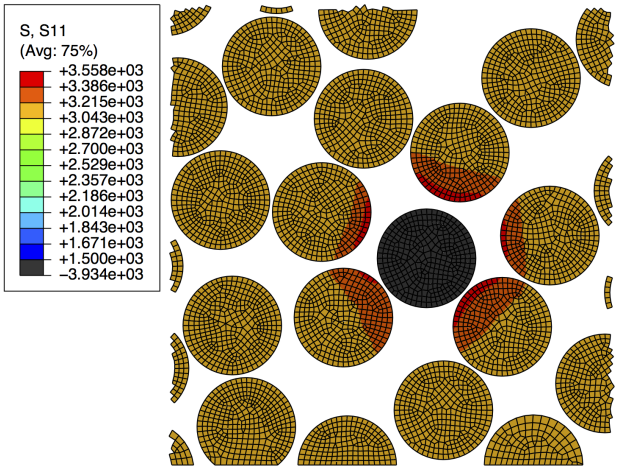


**Fig. 15** Stress concentrations in intact fibres surrounding a broken one (in black).

length. This effect is captured by the model, as shown in Figure 13. After a fibre breaks a crack in the matrix surrounding this broken fibre can appear, as shown in Figure 14. The crack progression is hampered by the intact surrounding fibres, that are affected by stress concentrations as shown in Figure 15. These stress concentrations act in a small region surrounding the broken fibre.

The first fibre failure is proceeded by the failure of other fibres. As previously stated, the break location is determined by flaws in the fibres. From the performed analysis it is seen that the majority of the fibres did not fail in the same plane, leading to the formation of a disperse cluster instead of a co-planar one. This type of cluster development has been reported previously in the literature [18, 24]. The locations of fibre breaks are represented in Figure 16 and it can be observed that many fibres are broken in multiple locations.

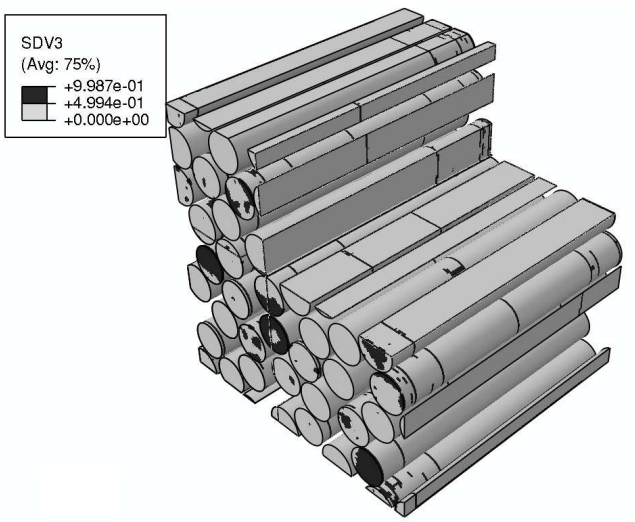


**Fig. 16** Location of fibre breaks after the failure of the composite: fracture zones represented in black.

From the shown analysis it is argued that the model captures the main failure mechanisms of polymer composites in longitudinal tension reported in the literature.

### 3.4 Results for the AS4-M50S carbon hybridization

This section focuses on the study of the hybridization between the AS4 and M50S carbon fibres previously addressed using the analytical models. The properties of the AS4 carbon fibres are shown in Table 4. For the M50S carbon fibres, due to lack of information, the same fibre properties were used, with the exception of the longitudinal Young's modulus, Weibull parameters and fibre radius [25] shown in Table 5.

**Table 5** M50S carbon fibre properties.

| Material property | Value |
|---|---|
| *Fibre diameter* | |
| $2R$ (mm) | 0.0053 |
| *Young's moduli* | |
| $E_1$ (MPa) | 480000 |
| *Weibull parameters* | |
| $\sigma_0$ (MPa) | 4600 |
| $m$ | 9 |
| $l_0$ (mm) | 10 |

Several RVEs were generated to study this hybridization. The tensile stress-strain curves are shown in Figure 17. All the RVEs studied had dimensions 15 times the radius of the fibre with higher diameter, leading to an RVE with a size equal to 52.5 $\mu$m. To study the effect

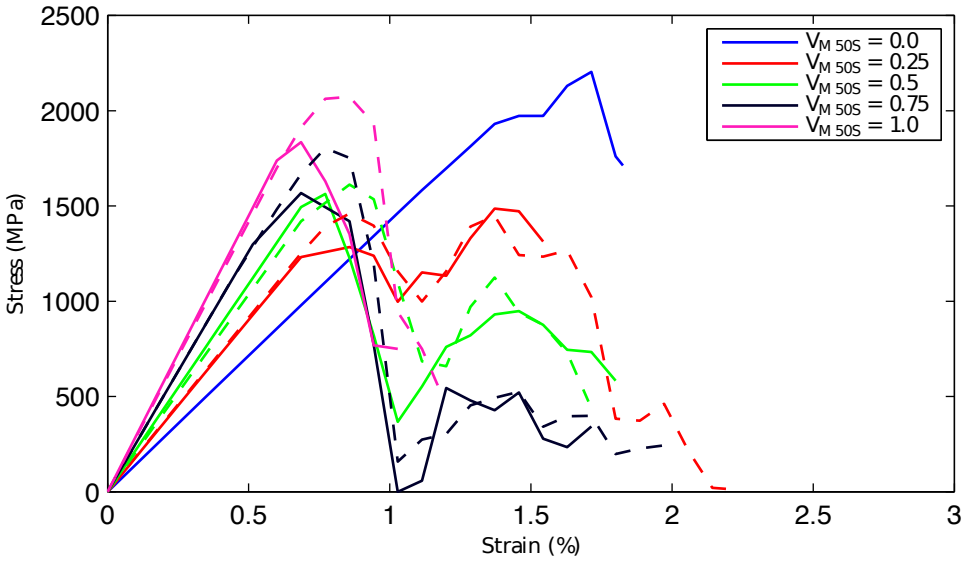


**Fig. 17** Stress-strain diagrams for AS4-M50S hybrid composites with various hybrid volume fractions: full - RVEs with all fibres with radius equal to 3.5 $\mu$m; dashed - RVE's with the M50S with radius equal to 2.65 $\mu$m.

of the fibre radius two types of RVEs were generated. The first consider both the AS4 and the M50S carbon fibres to have the same radius, equal to 3.5 $\mu$m; the corresponding results are shown in solid lines in Figure 17. The second type of RVEs considered the fibres to have the real fibre radii and, therefore, the AS4 and the M50S were modelled with different radii. The results for these RVEs are shown in Figure 17 in dashed lines. In this figure it is shown the tensile behaviour for hybrid composites with different volume fraction of each fibre type. Those with the same volume fraction of each fibre type are presented with the same colour. Comparing the results for the RVE's with the same radii (solid line) and different radii (dashed line) it is observed that considering of the M50S to be equal to 2.65 $\mu$m, higher tensile strength is obtained, for all the hybrid volume fractions analysed. Varying the volume fraction of each fibre type drastically changes the response of the composite material. In all cases, there is no interaction in the failure of both fibre types, this is, all the LE fibres fail prior to the failure of any HE fibres. This causes the first load drop seen for all hybrid composites. However, as we increase the volume content of HE fibres the load drop is reduced, being minimum for a volume fraction of M50S fibres equal to 0.25 (curves in red).

The stress-strain curves for the hybrid composite with a volume fraction of M50S fibres equal to 0.25 are again shown in Figure 18 alongside the microstructure of the RVE, where the circles in full represent broken fibres while the others represent intact fibres. Analysing the microstructures it is possible to note that all the LE fibres (M50S fibres) fail prior to the failure of a single

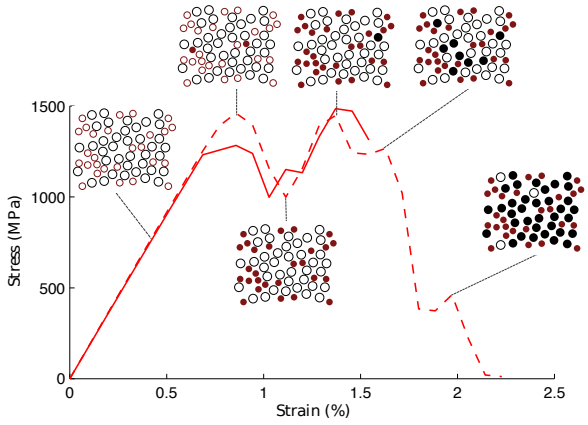


**Fig. 18** Stress-strain curves and microstructures for the hybrid composite with a volume fraction of M50S carbon fibres equal to 0.25: circles in full represent broken fibres.

high elongation fibre. This failure causes the first load drop seen in the curves. After the first load drop, as the HE fibres are still intact, the material is still able to carry stress which causes the increase in load after the first drop. At the second load peak, the failure strain of the HE has been reached which causes their failure and the failure of the material. Between both load peaks it is seen that, usually, the LE fibres keep on fracturing leading to the fragmentation of these fibres in multiple locations, which is responsible for the non-linearities seen between the failure of the LE and HE fibres. The tensile response for this hybridization is close to what is described as pseudo-ductility, for a volume fraction of

M50S fibres equal to 0.25, however, there is a small load drop after the failure of the LE fibres and prior to the failure of the HE fibres, typical of hybrid composites.

Having analysed the results from the micromechanical model for the hybridization between the AS4 and the M50S fibres it is useful to make the comparison between these results and the ones obtained with the composite damage model presented in Section 2.2. This comparison can be seen in Figure 19 for both AS4 and M50S non-hybrid composites and the hybrid composite with a volume fraction of M50S fibres equal to 0.25. From the presented results it is possible to conclude that the composite damage model clearly over predicts the results from the micromechanical model. These results are expected as it is seen that the global load sharing models, such as the one presented in Section 2.2, over predict the experimental results, as what drives the failure are local effects.

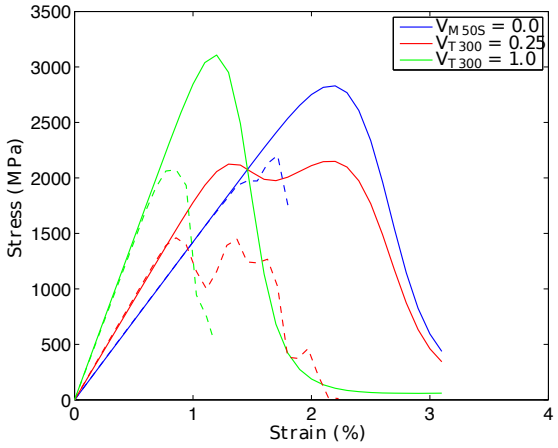


**Fig. 19** Comparison of the results from the micromechanical model (dashed lines) with the composite damage model (solid lines) for the AS4 and M50S hybridization.

### 3.5 Results for the AS4-T300 carbon hybridization

The tensile response for the hybridization of the AS4 carbon fibres and the T300 carbon fibres [5, 20], whose properties are shown in Table 6, is studied.

The T300 carbon fibres have a lower Weibull modulus and therefore a higher variability in fibre strength. Furthermore, the failure strain distribution of the T300 carbon fibres is closer to that of the AS4 carbon fibres than that of the M50S fibres (Figure 6), which can reduce the load drop seen for the AS4-M50S hybrids. The same RVE's generated for the previous hybridization with all fibres with radius equal to 3.5 $\mu$m were used for this hybridization, leading to the results shown in Figure 20.

**Table 6** T300 carbon fibre properties.

| Material property | Value |
|---|---|
| *Fibre diameter* | |
| $2R$ (mm) | 0.007 |
| *Young's moduli* | |
| $E_1$ (MPa) | 232000 |
| $E_2$ (MPa) | 15000 |
| *Poissons ratio* | |
| $\nu_{12}$ | 0.2 |
| *Shear moduli* | |
| $G_{12}$ (MPa) | 15000 |
| $G_{23}$ (MPa) | 7000 |
| *Coefficients of thermal expansion* | |
| $\alpha_{11}$ ($^{\circ}C^{-1}$) | $-0.7 \times 10^{-6}$ |
| $\alpha_{22}$ ($^{\circ}C^{-1}$) | $12 \times 10^{-6}$ |
| *Critical energy release rate* | |
| $G_{ff}$ (N/mm) | $4 \times 10^{-3}$ |
| *Weibull parameters* | |
| $\sigma_0$ (MPa) | 3170 |
| $m$ | 5.1 |
| $l_0$ (mm) | 25 |

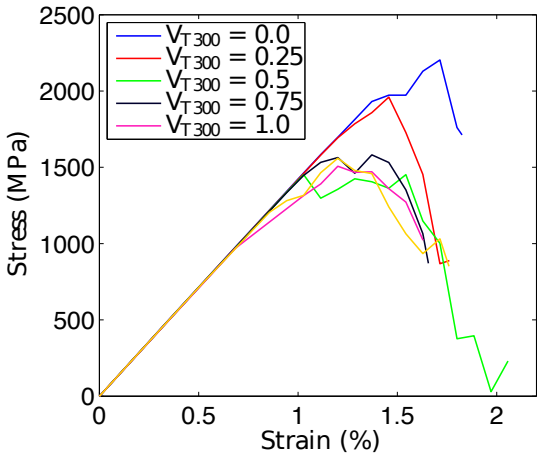


**Fig. 20** Stress-strain diagrams for AS4-T300 hybrid composites with various hybrid volume fractions.

Analysing this figure it is possible to see that the results for the AS4-T300 hybridization are quite different from those obtained using AS4-M50S hybridization. This is in agreement with the results obtained from the analytical models previously described. The more interesting results are for the hybrid composites with a volume fraction of T300 fibres equal to 0.5 and 0.75. For these hybrids there is a delay in first fibre failure in comparison to the non-hybrid T300 composite, which occurs at a strain equal to 0.7%. This can be attributed

to the reduction of the volume of T300 carbon fibres by replacing them with AS4 fibres, which reduces the probability of existence of a very severe defect in a fibre, causing the delay in first fibre failure. It is also possible to see there is no major stress drop due to the failure of the LE fibres in these hybrids. This is attributed to the higher dispersion in fibre strength of the T300 carbon fibres, which causes them to fail at different strains and, therefore, cause a more gradual failure. This can be seen in the microstructures shown in Figure 21 for the hybrid composite with a volume fraction of T300 fibres equal to 0.5. It is also possible to see that not all LE (T300) fibres fail before the HE (AS4) fibres start to fail, which leads to the gradual failure response shown. However, it should be noted that the fact that the increased strength dispersion of the T300 fibres increases the dispersion in the results, as they are quite dependent on the location and extension of the defects in the fibres.

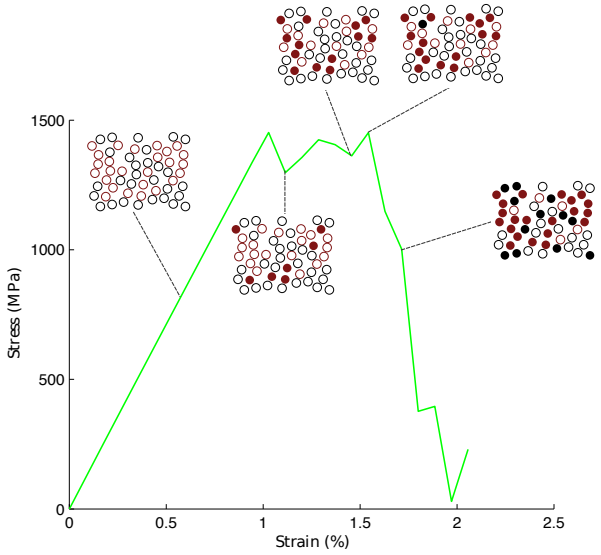


**Fig. 21** Stress-strain curve and microstructures for the hybrid composite with a volume fraction of T300 carbon fibres equal to 0.5: circles in full represent broken fibres.

Similar results are seen for the hybrid composite with a volume fraction of T300 carbon fibres equal to 0.75. The microstructures and stress-strain curves are shown in Figure 22. It is possible to see that the failure strain of the LE fibres differs from fibre to fibre due to the low Weibull modulus and high strength dispersion. Once again, there is the failure of HE fibres prior to the complete failure of the LE fibres, which might be key to the achievement of pseudo-ductility.

It is possible to conclude that the fibre strength distributions play a big role to achieve pseudo-ductility.

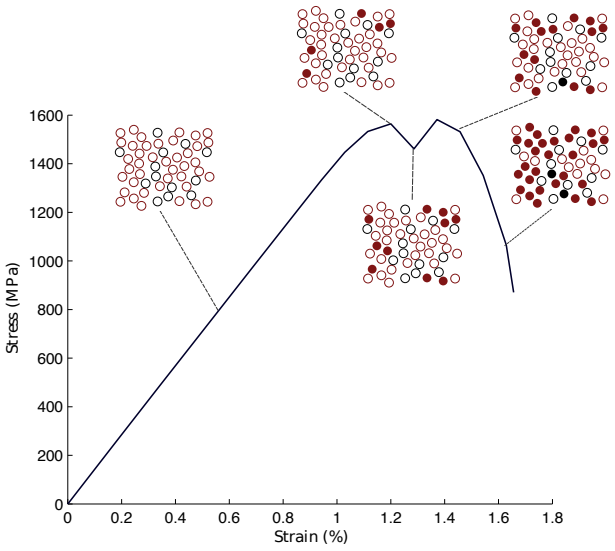


**Fig. 22** Stress-strain curve and microstructures for the hybrid composite with a volume fraction of T300 carbon fibres equal to 0.75: circles in full represent broken fibres.

The interaction between the failure of the LE and HE fibres is the key point for achieving pseudo-ductility.

## 4 Conclusion

An extensive analytical and numerical study on the effects of hybridization on the tensile failure of composite materials has been presented. Three different models with increasing complexity were developed. A model for dry tow failure, based on the statistics of fibre strength, identifies the effects of the fibres' statistical properties on the tensile response of non-interacting groups of fibres. From this model it was concluded that to achieve a progressive tow failure a continuity in the strength distributions of both fibre types is needed. Otherwise, sudden load drops, usually seen in hybrid composites, occur after the failure of the LE fibres.

An analytical model for composite materials was developed with the objective of bridging the gap between the model for dry tows and composite materials. This model is based on the single fibre fragmentation phenomenon and takes into account the presence of the matrix phase in the composite. It was observed that the matrix, namely, the matrix-fibre interface plays an important role in the tensile response of composite materials and that the results obtained for dry tows cannot be directly extrapolated for composite materials.

The last model developed was a micromechanical model that takes into account the fibre strength variability, and it is able to capture the main failure mechanisms in unidirectional composite materials. From this

model it was possible to establish the failure sequence in unidirectional composites, which was seen to be similar to what was previously reported in the literature. For hybrid composites it was possible to determine the complete tensile response of the composite, including the load drop after the failure of the LE fibres and the second load drop due to the failure of the HE fibres. It was concluded that the Weibull modulus plays a critical role in the catastrophic failure of composites. A lower Weibull modulus, higher strength variability, leads to a more gradual failure, that in conjunction with the failure of the HE fibres prior to the complete failure of the LE fibres are the key parameters to achieve pseudo-ductility. test

## References


1. Arteiro A, Catalanotti G, Melro A, Linde P, Camanho P (2014) Micro-mechanical analysis of the in situ effect in polymer composite laminates. Composite Structures 116:827 – 840, DOI http://dx.doi.org/10.1016/j.compstruct.2014.06.014
2. Bažant Z, Oh B (1983) Crack band theory for fracture of concrete. Matériaux et Construction 16(3):155–177, DOI 10.1007/BF02486267
3. Benzeggagh M, Kenane M (1996) Measurement of mixed-mode delamination fracture toughness of unidirectional glass/epoxy composites with mixed-mode bending apparatus. Composites Science and Technology 56(4):439 – 449, DOI http://dx.doi.org/10.1016/0266-3538(96)00005-X
4. Curtin W (1991) Exact theory of fibre fragmentation in a single-filament composite. Journal of Materials Science 26(19):5239–5253, DOI 10.1007/BF01143218
5. Curtin WA, Takeda N (1998) Tensile strength of fiber-reinforced composites: II. Application to polymer matrix composites. Journal of Composite Materials 32(22):2060–2081
6. Fiedler B, Hojo M, Ochiai S, Schulte K, Ando M (2001) Failure behavior of an epoxy matrix under different kinds of static loading. Composites Science and Technology 61(11):1615–1624
7. Foray G, Descamps-Mandine A, R'Mili M, Lamon J (2012) Statistical flaw strength distributions for glass fibres: Correlation between bundle test and afm-derived flaw size density functions. Acta Materialia 60(9):3711 – 3718
8. Fukuda H (1984) An advanced theory of the strength of hybrid composites. Journal of Materials Science 19(3):974–982, DOI 10.1007/BF00540468
9. Ibnabdeljalil M, Curtin W (1997) Strength and reliability of fiber-reinforced composites: Localized load-sharing and associated size effects. International Journal of Solids and Structures 34(21):2649 – 2668, DOI http://dx.doi.org/10.1016/S0020-7683(96)00179-5
10. Jr LM, Dai G (2014) Hybrid carbon/glass fiber composites: Micromechanical analysis of structure–damage resistance relationships. Computational Materials Science 81(0):630 – 640, DOI http://dx.doi.org/10.1016/j.commatsci.2013.08.024
11. Kelly A, Tyson W (1965) Tensile properties of fibre-reinforced metals: Copper/tungsten and copper/molybdenum. Journal of the Mechanics and Physics of Solids 13(6):329 – 350, DOI http://dx.doi.org/10.1016/0022-5096(65)90035-9
12. Martínez X (2008) Micro-mechanical simulation of composite materials using the serial/parallel mixing theory. PhD thesis, Ph. D. thesis, Departament de Resistència de Materials i Estructures a l'Enginyeria (RMEE)—UPC. Director: Sergio Oller
13. Melro A, Camanho P, Pinho S (2008) Generation of random distribution of fibres in long-fibre reinforced composites. Composites Science and Technology 68(9):2092 – 2102, DOI http://dx.doi.org/10.1016/j.compscitech.2008.03.013
14. Melro A, Camanho P, Pires FA, Pinho S (2013) Micromechanical analysis of polymer composites reinforced by unidirectional fibres: Part I - constitutive modelling. International Journal of Solids and Structures 50(11–12):1897 – 1905, DOI http://dx.doi.org/10.1016/j.ijsolstr.2013.02.009
15. Melro A, Camanho P, Pires FA, Pinho S (2013) Micromechanical analysis of polymer composites reinforced by unidirectional fibres: Part II - micromechanical analyses. International Journal of Solids and Structures 50(11–12):1906 – 1915, DOI http://dx.doi.org/10.1016/j.ijsolstr.2013.02.007
16. Rajan VP, Curtin WA (2015) Rational design of fiber-reinforced hybrid composites: A global load sharing analysis. Composites Science and Technology 117:199 – 207, DOI http://dx.doi.org/10.1016/j.compscitech.2015.06.015
17. Scott A, Sinclair I, Spearing S, Thionnet A, Bunsell A (2012) Damage accumulation in a carbon/epoxy composite: Comparison between a multiscale model and computed tomography experimental results. Composites Part A: Applied Science and Manufacturing 43(9):1514 – 1522, DOI http://dx.doi.org/10.1016/j.compositesa.2012.03.011
18. Scott A, Sinclair I, Spearing S, Thionnet A, Bunsell A (2012) Damage accumulation in a carbon/epoxy composite: Comparison between a multiscale model and computed tomography experimental results. Composites Part A: Applied

Science and Manufacturing 43(9):1514 – 1522, DOI http://dx.doi.org/10.1016/j.compositesa.2012.03.011
19. Simulia DS (2012) Abaqus 6.12 documentation. Providence, Rhode Island, US
20. Soden P, Hinton M, Kaddour A (1998) Lamina properties, lay-up configurations and loading conditions for a range of fibre-reinforced composite laminates. Composites Science and Technology 58(7):1011 – 1022, DOI http://dx.doi.org/10.1016/S0266-3538(98)00078-5
21. Swolfs Y, Gorbatikh L, Verpoest I (2014) Fibre hybridisation in polymer composites: A review. Composites Part A: Applied Science and Manufacturing 67(0):181 – 200, DOI http://dx.doi.org/10.1016/j.compositesa.2014.08.027
22. Swolfs Y, McMeeking R, Rajan V, Zok F, Verpoest I, Gorbatikh L (2015) Global load-sharing model for unidirectional hybrid fibre-reinforced composites. Journal of the Mechanics and Physics of Solids pp JMPSD1400,292 –, DOI http://dx.doi.org/10.1016/j.jmps.2015.08.009
23. Swolfs Y, McMeeking RM, Verpoest I, Gorbatikh L (2015) The effect of fibre dispersion on initial failure strain and cluster development in unidirectional carbon/glass hybrid composites. Composites Part A: Applied Science and Manufacturing 69(0):279 – 287, DOI http://dx.doi.org/10.1016/j.compositesa.2014.12.001
24. Swolfs Y, Morton H, Scott A, Gorbatikh L, Reed P, Sinclair I, Spearing S, Verpoest I (2015) Synchrotron radiation computed tomography for experimental validation of a tensile strength model for unidirectional fibre-reinforced composites. Composites Part A: Applied Science and Manufacturing 77:106 – 113, DOI http://dx.doi.org/10.1016/j.compositesa.2015.06.018
25. Tanaka F, Okabe T, Okuda H, Kinloch IA, Young RJ (2014) Factors controlling the strength of carbon fibres in tension. Composites Part A: Applied Science and Manufacturing 57(0):88 – 94, DOI http://dx.doi.org/10.1016/j.compositesa.2013.11.007
26. Turon A, Costa J, Maimí P, Trias D, Mayugo J (2005) A progressive damage model for unidirectional fibre-reinforced composites based on fibre fragmentation. part I: Formulation. Composites Science and Technology 65(13):2039 – 2048, DOI http://dx.doi.org/10.1016/j.compscitech.2005.04.012
27. Varna J, Berglund L, Ericson M (1997) Transverse single-fibre test for interfacial debonding in composites: 2. modelling. Composites Part A: Applied Science and Manufacturing 28(4):317 – 326, DOI http://dx.doi.org/10.1016/S1359-835X(96)00125-X
28. Weibull W (1951) A statistical distribution function of wide applicability. Journal of Applied Mechanics - Transactions of the ASME 58(7):1001–1010
29. Zweben C (1977) Tensile strength of hybrid composites. Journal of Materials Science 12(7):1325–1337, DOI 10.1007/BF00540846